Detection of dedifferentiated stem cells in *Drosophila* testis

Muhammed Burak Bener[1], Boris M. Slepchenko[1, 2*] and Mayu Inaba[1*]

1. Department of Cell Biology, University of Connecticut Health, Farmington, CT 06030
2. Richard D. Berlin Center for Cell Analysis and Modeling, University of Connecticut School of Medicine, Farmington, CT 06030

[*] Correspondence: inaba@uchc.edu, boris@uchc.edu

Abstract

Tissue homeostasis relies on the stable maintenance of the stem cell pool throughout an organism's lifespan. Dedifferentiation, a process in which partially or terminally differentiated cells revert to a stem cell state, has been observed in a wide range of stem cell systems, and it has been implicated in the mechanisms for stem cell maintenance. Dedifferentiated stem cells are morphologically indistinguishable from original stem cells, making them challenging to identify. Therefore, whether dedifferentiated stem cells have any distinguishable characteristics compared with original stem cells is poorly understood. The *Drosophila* testis provides a well-established model to study dedifferentiation. While our previous live imaging analyses have identified dedifferentiation events constantly occurring at steady state, existing genetic marking methods fail to detect most of the dedifferentiated stem cells and thus significantly underestimate the frequency of dedifferentiation events. Here, we established a genetic tool with improved sensitivity and used live imaging and mathematical modeling to evaluate the system. Our

findings indicate that the specificity of lineage-specific promoters is critical for successfully identifying dedifferentiated stem cells.

Introduction

Tissue homeostasis and repair rely on a stable stem cell pool, and deficiencies in stem cells lead to tissue degeneration, dysfunction and disease. Therefore, it is essential to maintain the stem cell pool throughout the lifespan of an organism. Dedifferentiation, where partially or terminally differentiated cells revert to the stem cell state, is one mechanism proposed to support stem cell maintenance across various tissues during both steady-state and regeneration conditions [1-9]. Given its role in stem cell maintenance, studying dedifferentiation and identifying dedifferentiated stem cells is essential. However, the underlying mechanisms of dedifferentiation remain poorly understood.

A key challenge in identifying dedifferentiated stem cells is that they are often morphologically and molecularly similar to the original stem cells [4]. Genetic marking, such as a lineage tracing technique, has been employed to distinguish dedifferentiated stem cells from the original stem cells [3-5, 10-14]. Genetic marking often relies on promoters active in differentiated cells, but not in stem cells, to induce recombination of reporter cassettes, resulting in the permanent marking of these cells. Ideally, recombination should remain completely silent in stem cells while being sufficiently high in targeted cells for accurate marking. However, this has been proven to be difficult because many cell-stage-specific markers exhibit overlapping expression across stages (reviewed in [2]), resulting in either leaky reporter activation in stem cells due to basal recombinase expression or insufficient reporter activation in differentiating cells, reducing the accuracy of tracing tools [15].

46 The *Drosophila* testis serves as an excellent model for studying *in vivo* stem cell
47 maintenance [16]. Each testis contains 8 to 12 germline stem cells (GSCs) around a cluster of
48 post-mitotic cells called the hub [17]. GSCs typically divide asymmetrically, producing one
49 daughter cell that remains attached to the hub and retains its stem cell identity, while the other
50 daughter cell is detached from the hub (called gonialblasts or GBs) and starts the differentiation
51 process [18]. A GB undergoes four rounds of mitosis to form cysts of 2-, 4-, 8-, and 16-cell
52 spermatogonia (SG) [19].

53 Dedifferentiation can be experimentally induced using forced differentiation of stem cells
54 in *Drosophila* testis. When the differentiation factor, Bag of Marbles (Bam), is temporarily
55 expressed, all GSCs start differentiation and physically leave the hub. After the treatment, cells
56 detached from the hub start migrating back to the hub and regaining stem cell identity [1]. This
57 phenomenon was first described by Brawley et al., in 2004 [1]. However, how frequently
58 dedifferentiation occurs under steady-state conditions is still unclear.

59 Current genetic marking tools detect dedifferentiated GSCs at low frequencies [10, 11].
60 All previous tools utilized the bamGal4 driver to drive FLP recombinase (UAS-FLP) expression
61 and permanently mark differentiating cells (Figure 1B-D). The low efficiency of marking is
62 likely due to the delay of FLP expression, which may not reach the threshold for effective
63 recombination until the 4-cell SG stage or later. Since GBs are the primary source of
64 dedifferentiation [9], such delay significantly affects the marking efficiency. Consequently, these
65 existing tools may fail to capture dedifferentiated GSCs across the fly's lifespan fully [10, 11].

66 In this study, we aimed to develop tools to improve efficiency. Specifically, we utilized
67 FLP directly driven by the Bam promoter combined with FRT-flanked cassettes. We tested two
68 FRT cassettes, each exhibiting a distinct threshold sensitivity to FLP dose. To evaluate the

69 efficiency and specificity of this system, we conducted long-term live imaging. We found that
70 the new FLP transgene has better efficiency, albeit with incomplete marking of dedifferentiated
71 stem cells in the *Drosophila* testicular niche.
72
73 **Results**
74
75 **Improvement of genetic marking system for identifying dedifferentiated GSCs.**
76 In our previous study, we investigated the mechanisms of GSC replenishment in the
77 *Drosophila* testis niche under steady-state conditions using long-term live imaging (~16 hours)
78 [9]. Among all the events observed in the niche (~6 total events per recording), 72% were
79 asymmetric cell division (ACD), 14% were losses (symmetric differentiation or stem cell loss
80 without division), 4% were symmetric renewal, and 10% were dedifferentiation (Figure 1A).
81 Given this 10% dedifferentiation rate observed over 16-hour imaging period (~0.6
82 dedifferentiation events per recording), we estimate that roughly ~1 GSC will be supplied via
83 dedifferentiation every day [9].
84 Previous studies have employed lineage-tracing tools to detect dedifferentiated GSCs [10,
85 11]. These systems rely on bamGal4-driven Flippase (FLP) expression that removes FRT-
86 flanked stop codons located between the promoter and the downstream reporter coding sequence.
87 When FLP-recombined cells dedifferentiate and become GSCs, these cells will be positive for
88 LacZ or GFP [10, 11]. We first tested this previous system using nos-FRT-mCherry-stop-FRT-
89 Gal4 cassette with UAS-GFP (hereafter referred to as nos>>GFP). On average, GFP-positive
90 GSCs comprised only approximately 10% of the total GSC pool at 28 days post-eclosion (Figure
91 1B-D), similar to the previous report (~14% shown in [11]). Considering the frequency observed

92 in live imaging (1~2/day [9]), this system might miss most dedifferentiation events. We
93 speculate that this issue was likely due to delays in FLP expression when the Gal4/UAS binary
94 system was used. Therefore, we sought to establish a new system.
95 To improve marking efficiency, we generated a transgenic fly to express FLPD5 (an FLP
96 variant with enhanced activity [20]) directly driven by the Bam promoter so that we can bypass
97 the Gal4-mediated UAS induction to minimize delays in inducing FLP recombinase activity
98 (Figure 1E).
99
100 **Bam-FLPD5 causes spontaneous flipping events in GSCs, which obscures dedifferentiation**
101 **marking.**
102 The newly established Bam-FLPD5 transgene showed a high frequency of GFP-positive
103 cells after introducing the same nos>>GFP reporter cassette as in the previous system (Figure
104 2A-D). To evaluate whether the marked GFP-positive GSC frequency reflects the
105 dedifferentiation rate, we conducted long-term live imaging of the niche to monitor GFP
106 activation. Testes expressing both the Bam-FLPD5, nos>>GFP, and Vasa-mCherry (a germline
107 cell marker) were imaged for approximately 12 hours using a z-stack to cover the entire niche. In
108 27 niches, each imaged for 12 hours, we observed eleven GSCs becoming GFP positive within
109 the niche (Figure 2E, Movie S1), even though the Bam promoter used to drive FLP expression
110 was expected to be active specifically in GB/SGs and not in GSCs. This is likely due to a
111 leaky/nonspecific driver activity in GSCs, resulting in unintended flipping events. Within the
112 same time period, the number of GB/SGs that became GFP-positive was twelve, indicating
113 almost no difference in the frequency of flipping events in the GSC and GB/SG pools. Given the
114 near-equal Bam-FLPD5 activity in GSC and GB/SG populations, we conclude that the majority

115 of the GFP-positive GSCs were not generated by dedifferentiation events, and therefore this
116 system is unsuitable for tracing dedifferentiated cells.
117
118 **UAS-FRT-stop-FRT-mCD8-GFP cassette shows reduced spontaneous flipping rate in**
119 **GSCs.**
120 We next strategized to overcome the issue of the nonspecific marking. Since the activity
121 of Bam promoter in GSCs is expected to be weak [21, 22], Bam-FLPD5 likely yields low levels
122 of FLP recombinase in the stem cells in the niche. On the other hand, the substrate constructs
123 with FRT sites may differ in their sensitivity to FLP recombinase activity [15]. Therefore, we
124 attempted to use an alternative reporter cassette with a higher threshold for FLP mediated
125 recombination to minimize spontaneous GFP activation in GSCs, so that it responds linearly to
126 FLP activity differences.
127 First, to test the recombination rates of different FRT cassettes, we compared the
128 recombination frequency of nos>>GFP to an alternative UAS-FRT-stop-FRT-mCD8-GFP,
129 together with nosGal4 (hereafter referred to as nos>>mCD8GFP) using heat-shock activatable
130 promoter-FLP (hs-FLP). We performed a single 30-min heat-shock treatment at 37°C to induce
131 FLP expression, then examined GFP positive GSC frequency after 24 hours [23, 24]. The
132 nos>>mCD8GFP yielded a significantly lower percentage of GFP-positive GSCs than
133 nos>>GFP indicating that nos>>mCD8GFP has a higher threshold to FLP and may be a good
134 candidate for Bam-FLPD5 substrate for marking of dedifferentiated cells (Figure S2A-C).
135 Then, we examined the frequency of GFP-positive GSCs using a combination of Bam-
136 FLPD5 and nos>>mCD8GFP and found that it indeed marks GSCs at a lower rate (Figure 3A-C)
137 than the Bam-FLPD5, nos>>GFP system (Figure 2D). To assess the recombination rate of Bam-

138 FLPD5 with nos>>mCD8GFP cassette in GSCs and in GB/SGs, we again employed a live
139 imaging approach. During imaging, we observed frequent GFP activation in differentiating cells,
140 including twelve GBs and four SGs, across 25 niches imaged for ~12 hours each (Figure 3D,
141 Movie S2). Notably, from these 25 recordings, we observed only one instance of GFP activation
142 that occurred in GSCs without prior dedifferentiation events (Figure 3D).
143 The observed reduction in spontaneous GFP activation in GSCs and efficient GFP
144 activation in GB/SGs suggests that the Bam-FLPD5 in combination with nos>>mCD8GFP
145 detects differentiating cells with higher specificity.
146
147 **Quantifying specificity and efficiency of lineage marking**
148 To estimate the number of GFP-positive cells that reflect true dedifferentiation events, we
149 formulated a computational model using observed rates of key cellular processes in our previous
150 live imaging study, including: asymmetric division (p), symmetric self-renewal (q), symmetric
151 differentiation (r), dedifferentiation (k_{dd}). Then, we defined flippase recombination rate in
152 GB/SGs to be (α) and recombination occurring in GSCs (α*) as the spontaneous background
153 event, disregarding stage-specific promoter activity. Because this background recombination
154 must also occur at the same rate in GB/SGs, the stage-specific recombination rate in GB/SGs
155 (α^{True}) is determined as ($\alpha^{True} = \alpha - \alpha^*$) (all rates are per cell cycle, Figure S1A, B).
156 Using a publicly available software *Virtual Cell (*VCell*)* [25, 26], we first simulated the
157 time-dependent changes in the fraction of GFP-positive GSCs and validated the model by fitting
158 the curve to the experimentally observed GFP rates. For the data obtained by using both
159 nos>>GFP and nos>>mCD8GFP cassettes, the model outputs closely matched the experimental
160 data (Figure 4A, B), yielding values of α* that are consistent with the estimates obtained directly

161 from the experimental data, see methods section "Estimation of flippase recombination rate in
162 GSCs (α*)" for details. These validate the model and indicate its ability to accurately recapitulate
163 the frequency of marked cells in the niche.
164
165 **Stage specificity of the recombination determines the feasibility of the detection system**
166 We next used the model to estimated how many of GFP positive cells are true
167 dedifferentiation cells. When the nos>>GFP cassette was used, spontaneous flippase
168 recombination in GSCs occurs at a rate nearly equal to the flippase recombination in GB/SGs,
169 α* ≈ α, indicating that the flippase activity is entirely not stage specific. In this case, the model
170 revealed that dedifferentiation rate k_{dd} had no discernible effect on the frequency of GFP-
171 positive GSCs, as expected. Indeed, the predicted frequency of GFP-positive GSCs remained
172 essentially same across a range of k_{dd} values (0, 0.1, and 0.2) (Figure 4C), indicating that the
173 observed GFP-positive rate is not reporting the dedifferentiation rate at all.
174 In contrast, when nos>>mCD8GFP cassette was used, which has a significantly lower
175 flippase recombination rate in GSCs than in GB/SGs, α*<< α, the GFP positive rate showed the
176 clear sensitivity to the dedifferentiation rate k_{dd}, as the percentage of GFP-positive GSCs
177 significantly increases with the increasing k_{dd} (Figure 4D). These results highlight the
178 importance of the stage specificity of flippase excision events in marking the cells for estimating
179 dedifferentiation frequency.
180 An important aspect of lineage tracing is distinguishing true lineage-marked cells from
181 those marked due to non-specific flipping events (false positives). The model estimates the rate
182 of 'false positives' as GFP-positive GSCs originating from two sources: 1) GSCs that
183 spontaneously activate GFP within the niche and 2) dedifferentiated GFP-positive GSCs whose

184 lineage traces back to a spontaneous GFP activation event within and outside the niche. With the
185 Bam-FLPD5, nos>>GFP system, the model revealed that essentially all (~100%) of the observed
186 GFP-positive GSCs at all time points were false positives (Figure 4E, green line). In contrast,
187 with the nos>>mCD8GFP cassette, the fraction of false positives was reduced to about 45%
188 across all time points (Figure 4E, orange line). While still substantial, this represents a significant
189 improvement over the Bam-FLPD5, nos>>GFP system.

190 To further explore the relationship between the stage specificity of the flipping event and
191 false positive rates, we systematically varied the "flipping" ratio (α^*/α^{True}) – the ratio of
192 background flippase activity in GSCs (α^*) to the stage-specific activity in GB/SGs (α^{True}) –
193 while keeping other parameters constant. We performed this analysis at a representative time
194 point (t=12 cycles), given that the probability of false positives is largely time-independent
195 (Figure 4E). As expected, low flipping ratios yield low false-positive rates approaching 0, but as
196 the flipping ratio increases, the probability of false grows rapidly, showing a sigmoid semi-log
197 dependence (Figure 4F). These findings indicate that minimizing background flippase activity is
198 a critical factor for the genetic marking system to be successful.

199 In summary, our modeling analysis demonstrates that the Bam-FLPD5, nos>>mCD8GFP
200 system reports dedifferentiation rates much more efficiently than the previous system, although
201 approximately half of the GFP positive GSCs are still false positives. The expected "true"
202 dedifferentiation rate, assuming zero background recombination in GSCs, and 100%
203 recombination in GB/SGs, is represented by the blue line in Figure 4B. This curve indicates that
204 the dedifferentiated cells rapidly occupy the entire niche within ~14 days of fly's age (Figure
205 4B). The difference between the blue and orange curves represents the false negative rate that
206 needs to be improved in future studies.

207

208 **Experimentally increasing the dedifferentiation rates results in a high frequency of marked**

209 **GSCs**

210 To experimentally test the model's predicted sensitivities to dedifferentiation, we

211 introduced a heat-shock-inducible Bam (hs-Bam) transgene into flies carrying either the Bam-

212 FLPD5, nos>>GFP or Bam-FLPD5, nos>>mCD8GFP lineage marking system. The hs-Bam

213 transgene is commonly used to induce dedifferentiation; a heat-shock treatment temporarily

214 forces GSCs to differentiate, and when treatment stops, GSCs are replenished through

215 dedifferentiation [27].

216 Our model predicts that the Bam-FLPD5, nos>>GFP system, with its high α^*/α^{True} ratio,

217 would be insensitive to changes in k_{dd} (Figure 4C), while the Bam-FLPD5, nos>>mCD8GFP

218 system, with its lower α^*/α^{True} ratio, would show an increase in GFP-positive GSCs with

219 increasing k_{dd} (Figure 4D).

220 At 7 days after eclosion, we observed a significant increase in GFP-positive GSCs in flies

221 carrying the hs-Bam transgene with the Bam-FLPD5, nos>>mCD8GFP system (Figure 5A, B,

222 E). This is likely due to the basal activity of the heat-shock promoter at room temperature,

223 leading to continuous Bam expression. This continuous Bam expression causes GSC loss, which

224 subsequently induces the replacement events likely through dedifferentiation. Notably, this

225 increase in GFP-positive GSCs is consistent with the model's prediction that Bam-FLPD5,

226 nos>>mCD8GFP system is sensitive to changes in the dedifferentiation rate.

227 In contrast, and as predicted by our model, increasing dedifferentiation frequency in flies

228 carrying the hs-Bam transgene with Bam-FLPD5, nos>>GFP system, did not result in a

229 significant change in GFP-positive GSCs under the same conditions (Figure 5C-E). These data

230 suggest that the observed increase in GFP-positive GSCs in the Bam-FLPD5, nos>>mCD8GFP
231 system reflects the dedifferentiation events.
232 Interestingly, the standard heat-shock protocol to induce dedifferentiation with hs-Bam at
233 37°C followed by a 3 to 7-day recovery period, did not result in a significant change in GFP-
234 positive GSCs with both nos>>GFP and nos>>mCD8GFP cassettes (Figure S3). We speculate
235 that high levels of Bam production during heat-shock treatments may cause negative feedback
236 mechanisms that suppress transcription from the Bam promoter used for the FLPD5 (Bam-
237 FLPD5), thereby reducing the efficiency of marking differentiating cells.
238
239 **Discussion**
240 Lineage tracing is a powerful tool for tracking cellular dynamics *in vivo*, including
241 proliferation, differentiation, and dedifferentiation. Recombinase-based systems, such as Cre-
242 loxP and FLP-FRT are widely used in lineage tracing. However, their reliance on tissue-specific
243 promoters makes them susceptible to "leaky" or off-target recombination. Studies in mice have
244 demonstrated the non-specificity of various Cre lines [28, 29]. Ideally, a lineage-specific
245 promoter should be distinctly active ("ON") in one target lineage and inactive ("OFF") in all
246 other lineages.
247 In this study, we developed an enhanced genetic marking system (Bam-FLPD5) to
248 identify dedifferentiated GSCs with improved sensitivity. By addressing key limitations of
249 previous lineage tracing methods, including delayed reporter activation that reduces marking
250 efficiency, our Bam-FLPD5 system offers a more accurate approach for monitoring
251 dedifferentiation events. While genetic marking is a valuable tool for studying dedifferentiation,
252 live imaging remains essential for confirming these events and distinguishing them from artifacts

253 like spontaneous reporter activation in off-target cells. Several past studies have utilized live
254 imaging to observe stem cell dynamics in real time, including studies in mouse spermatogonial
255 stem cells [30], and *Drosophila* male GSCs [31]. Through real-time tracing of cells within intact
256 tissues, these studies have provided insights into cellular plasticity and ability of partially or
257 terminally differentiated cells to revert to a stem cell state. In this study, we integrated live
258 imaging with our genetic marking approach to further enhance the accuracy and provide an
259 additional layer of validation.

260 Our findings emphasize spontaneous recombination's significant and previously
261 underestimated impact on lineage tracing studies. Spontaneous recombination likely occurs in
262 other lineage tracing systems but has often been overlooked due to the lack of real-time
263 validation methods like live imaging. Our simulations showed a strong positive correlation
264 between the false positive rates and the FLP recombination ratio (α*/α) (Figure 4F). For
265 example, the Bam-FLPD5, nos>>GFP system, where the estimated α*/α ratio was ~1 (almost no
266 stage specificity of the recombination), our simulation showed essentially all of GFP-positive
267 GSCs (~100%) across 56 cycles are false positives as we expected. This suggests that none of
268 the observed GFP-positive GSCs in this system represent the true dedifferentiation events
269 (Figure 4E, green line). In contrast, the Bam-FLPD5, nos>>mCD8GFP system, with a lower
270 α*/α ratio, exhibited a reduced false positive rate of approximately 45% (Figure 4E, orange line),
271 implying that roughly 55% of GFP-positive GSCs likely represent true dedifferentiation. This
272 enables the use of this system to monitor the dedifferentiation rate for future studies.

273 Although our new genetic marking system improved the sensitivity of previously
274 established systems, it still does not capture all dedifferentiated cells. A comparison between the
275 observed percentages of dedifferentiated GSCs in the Bam-FLPD5 system (Figure 4B, blue bars)

276 and the expected curve derived from our mathematical model (Figure 4B, blue line), which
277 assumes 100% recombination efficiency in all differentiating cells, reveals that a large portion of
278 differentiating cells remains unmarked with currently achieved recombination efficiency. There
279 is still a need for further research focused on identifying gene promoters with both high activity
280 and high specificity.

281 With the advances in next-generation sequencing and single-cell technologies,
282 computational-based lineage tracing tools have emerged (reviewed in [32, 33]). These include
283 Polylox DNA barcoding, which uses Cre recombinase to create diverse combinations barcodes to
284 uniquely label cells of interest for lineage tracing (although promoter specificity of Cre
285 expression remains a consideration) [34, 35]. Other approaches leverage naturally occurring
286 somatic mutations, such as those in mitochondrial DNA (mtDNA) [36], or engineered mutations
287 introduced via CRISPR-Cas9 systems [37] to infer cellular relationships. While DNA barcoding
288 and marker-independent methods offer valuable insights, they often lack the ability to directly
289 validate the lineage tracing events in real-time. A key advantage of our approach is the
290 integration of long-term live imaging with genetic marking. This combination allows for direct
291 assessment of accuracy, a capability lacking in many newer techniques.

292 GSCs typically divide asymmetrically, with several intrinsic factors non-randomly
293 segregated between the stem cell and its differentiating daughter cell [38-40]. However,
294 dedifferentiation disrupts this intrinsic asymmetry, and whether this results in differences
295 between original and dedifferentiated stem cells is not well understood. Moreover,
296 dedifferentiated stem cells have been implicated as a cellular origin of tumorigenesis in several
297 tissues [41, 42]. Lineage tracing tools, such as the Bam-FLPD5 system developed in this study,
298 provide a valuable approach to investigate these questions.

299 **Materials and methods**

300

301 **Fly husbandry and strains**

302 Flies were raised on standard Bloomington medium at 25°C (unless temperature control was
303 required). 0- to 7-day-old adults were used for all experiments unless specific ages of flies were
304 noted. The following fly stocks were obtained from Bloomington Stock Center (BDSC); nosGal4
305 (BDSC64277) [43]; 20XUAS-FLPD5 (BDSC55805); UAS(FRT.stop)mCD8-GFP
306 (BDSC30032); hs-flp (BDSC1929) and hs-bam (BDSC24636). pVas-Vasa mCherry
307 (FBtp0065762) [44] was a kind gift from Yukiko Yamashita. nos-FRT-mCherry-stop-FRT-Gal4,
308 UAS-GFP [23] was from Inaba lab stock.

309

310 **Immunofluorescence staining**

311 Testes were dissected in 1x phosphate-buffered saline (PBS) (Fisher Scientific) and fixed in 4%
312 formaldehyde (Electron Microscopy Sciences) in PBS for 30 minutes. Following fixation, testes
313 were washed in PBS containing 0.2% TritonX-100 (Fisher Scientific) (PBST) for a minimum of
314 60 minutes (three washes of 20 minutes each). They were then incubated overnight at 4°C with
315 primary antibody in 3% bovine serum albumin (BSA) (Sigma) in PBST. The following day,
316 samples were washed in PBST for 60 minutes (three washes of 20 minutes each), incubated with
317 secondary antibody in 3% BSA in PBST at room temperature for 2 hours, and then washed again
318 in PBST for 60 minutes (three washes of 20 minutes each). Finally, samples were mounted using
319 VECTASHIELD with 4',6-diamidino-2-phenylindole (DAPI) (Vector Lab).
320 The primary antibodies used were as follows: rat anti-Vasa (1:20; developed by A. Spradling and
321 D. Williams, obtained from Developmental Studies Hybridoma Bank (DSHB); mouse anti-hu-li

322 tai shao (Hts) (1:20, 1B1; DSHB) and mouse-anti- Fasciculin III (FasIII) (1:40, 7G10; DSHB).
323 AlexaFluor-conjugated secondary antibodies (Abcam) were used at a dilution of 1:400.
324

325 **Long-term live imaging**

326 Long-term live imaging was conducted using a previously established method [31]. Testes were
327 dissected in 1X Becker Ringer's [31] solution and mounted onto 35mm Glass Bottom Dishes
328 (Nunc). To prepare the imaging dish, 500 µL of 1 mg/mL poly-L-lysine (Sigma) was applied to
329 the coverslip area of the dish and incubated at room temperature for 5- to 7-hours. Following
330 incubation, the poly-L-lysine solution was replaced with the Becker Ringer's solution. Testes
331 were then dissected in Becker Ringer's solution and mounted on the poly-L-lysine coated surface
332 with the tips oriented downward. Next, Becker Ringer's solution was carefully removed, and
333 pre-warmed (room temperature) Schneider's *Drosophila* medium (supplemented with 10% fetal
334 bovine serum and glutamine–penicillin–streptomycin, Sigma) was added to the dish.
335 Z-stack images were acquired at 2 µm intervals (10-15 stacks total) using the Zeiss LSM800
336 Airyscan microscope with a 63× oil immersion objective (NA = 1.4) every 10 minutes over a 16-
337 hour period. The preset tiling function was utilized for automated image acquisition.
338

339 **Image analyses**

340 Airyscan time-lapse images were processed with Zen software (Zeiss). Each z-stack was
341 manually analyzed to track cells, record their GFP-expression status, and identify
342 dedifferentiation events. The hub area was identified as a circular, autofluorescent region located
343 near the testis tip, surrounded by fluorescently labeled germline stem cells. Dedifferentiation
344 events were recorded when germline cells, initially positioned more than one cell layer away

345 from the hub's edge reattached to the hub and maintained their attachment for at least 30
346 minutes. The moment a dedifferentiated cell observed at the hub edge was marked as the
347 "reattachment" time point. Movies were annotated using Veed.io.
348
349 **Estimation of flippase recombination rate in GSCs (α*)**
350 The flippase recombination rate in GSCs (α*) was determined directly from live-imaging data.
351 For the BamFLPD5, nos>>GFP system, 27 testes were imaged for 12 hours each (Figure 2E).
352 Each testis contains an average of 9 GSCs. Across all testes, 11 GSCs were observed to become
353 GFP-positive during the imaging period. Therefore, α* was calculated by dividing the total
354 number of flipping events in GSCs (11) by the total number of GSC cell cycles observed (27
355 testes*9 GSCs/testis=243 GSC cycles), yielding a value of 0.045 flipping events per cell cycle. A
356 similar procedure was followed for the Bam-FLPD5, nos>>mCD8GFP system, using its
357 respective experimental data in Figure 3D. Here, α* was calculated by dividing the total number
358 of flipping events in GSCs (1) by the total number of GSC cell cycles observed (25 testes*9
359 GSCs/testis=225 GSC cycles), yielding a value of 0.004 flipping events per cell cycle.
360
361 **Short-term live imaging**
362 Short-term live imaging was performed for static image acquisition of testes to avoid potential
363 signal loss or loss of extracellularly located fluorescent protein (GFP) during fixation and
364 permeabilization. Dissected testes were placed in Schneider's Drosophila medium (supplemented
365 with 10% fetal bovine serum and glutamine–penicillin–streptomycin, Sigma), then placed onto
366 two etched rings on Gold Seal Rite-On Micro Slides with media and covered with coverslips. Z-
367 stack images were acquired at 1 μm intervals (15-20 stacks total) using the Zeiss LSM800

368 Airyscan microscope with a 63× oil immersion objective (NA = 1.4). For these short-term live
369 imaging experiments, all images were taken within 30 minutes of dissection, without time-lapse
370 imaging.
371
372 **GSC depletion and recovery**
373 GSC depletion and recovery were performed as previously described, with modifications [27].
374 Adult flies (0- to 3-days old) carrying the hs-Bam transgene (BDSC24636) were raised at 22°C.
375 They underwent six heat shock treatments in a 37°C water bath for 30 minutes, twice daily,
376 within vials with fly food. Between treatments, the vials were maintained in a 29°C incubator.
377 Following the last heat shock treatment, the flies were returned to 22°C for the recovery phase.
378 Testes were dissected after a 5-day recovery period.
379
380 **Generation of Bam-FLPD5 transgenic line**
381 The minimum bam promoter sequence (-198 to transcription start site, TSS) [45] was amplified
382 from genomic DNA isolated from wild-type flies using the following primers:
383 SphI KpnI bam -198 Forward: 5'-
384 AGCGGATCCAAGCTTGCATGCGGTACCCCAAATCAGTGTGTATAATT-3'
385 Bam -198 Reverse: 5'-TATTCTTAAGTTAAATCACACAAATCACTCGAT-3'
386 Separately, the FLPD5 sequence, excluding the PEST sequence, was amplified from the genomic
387 DNA of the 20XUAS-FLPD5 strain (BDSC55805) using the following primers:
388 FLPD5 Forward: 5'-
389 GTGATTTGTGTGATTTAACTTAAGAATAATGCCGCAGTTTGATATCCTCTG-3'

390 FLPD5 Reverse: 5'-GTACCCTCGAGCCGCTTAAATACGGCGATTGATGTAGGAGCTCA-
391 3'
392 pUAST-attB vector was digested by SphI and NotI restriction enzymes to remove the UASt
393 promoter. The amplified bam -198 and FLPD5 fragments were assembled with the digested
394 vector using a Gibson Assembly kit (NEB) and sequenced. Transgenic flies were generated using
395 strain attP2 by PhiC31 integrase-mediated transgenesis (BestGene).
396
397 **Mathematical modeling**
398
399 *Model*
400 The model was developed for the analysis of efficiency, specificity, and sensitivity of
401 genetic constructs designed for the identification of dedifferentiated germline stem cells (GSCs)
402 in *Drosophila* testes.
403 The model outputs must mimic experimental readouts - time-dependent fractions of
404 marked dedifferentiated GSCs. Correspondingly, we formulate our model in terms of numbers of
405 unmarked and marked GSCs in the niche and corresponding GBs and SGs available for
406 dedifferentiation in the vicinity of the niche. The stem cell pool is presented in the model by the
407 following variables: the number of the innate unmarked stem cells, $n_0(t)$; the number of the
408 dedifferentiated unmarked stem cells, $n_1(t)$; the number of the dedifferentiated stem cells
409 marked as a result of the promoter activation and subsequent flippase recombination, $n_2(t)$; and
410 the number of the stem cells marked by spontaneous nonspecific GFP activation (false positives),
411 $n_3(t)$. The GB/SGs pool is described by the following variables: the number of unmarked

GB/SGs, $m_1(t)$; the number of GB/SGs marked due to the promoter activation, $m_2(t)$; and the number of GB/SGs marked by spontaneous GFP activation, $m_3(t)$.

The variables described above are governed by the following key processes included in the model (Figure S1A,B): asymmetric division (characterized by rate constant p), symmetric renewal (q), symmetric differentiation/loss (r), dedifferentiation of GB/SGs (k_{dd}), differentiation of GB/SGs (β), flippase recombination in GB/SGs (α), flippase recombination in GSCs (α*), and stage-specific flippase recombination in GB/SGs (α^{True}) ($\alpha^{True} = \alpha - \alpha^*$) (all rates are per cell cycle).

We assume that the processes involving unmarked and marked cells are described by equivalent parameter values. We further assume that the niche tightly controls the total number of GSCs, $N = n_0(t) + n_1(t) + n_2(t) + n_3(t)$, so that it remains constant at all times,

$$n_0(t) + n_1(t) + n_2(t) + n_3(t) = N = const. \quad (1)$$

Experimental fractions of GFP-positive cells were obtained from the pools containing large numbers of cells for each time point (on the order of a hundred or more), so that the fluctuations of their averages were relatively small. This allowed us to ignore the discreteness of the variables and approximate the dynamics of the corresponding fractions, $s_i(t) = \frac{n_i(t)}{N}$, $i = 0,1,2,3$, and $g_j(t) = \frac{m_j(t)}{N}$, $j = 1,2,3$, by differential equations:

$$\begin{aligned} \partial_t s_0 &= -(r - q + \alpha^*)s_0 \\ \partial_t s_1 &= -(r - q + \alpha^*)s_1 + k_{dd}g_1, \\ \partial_t s_2 &= -(r - q)s_2 + k_{dd}g_2, \\ \partial_t s_3 &= -(r - q)s_3 + \alpha^*(s_0 + s_1) + k_{dd}g_3; \end{aligned} \quad (2)$$

and

$$\partial_t g_1 = \nu(s_0 + s_1) - (\alpha + \alpha^* + \beta + k_{dd})g_1,$$

$$\partial_t g_2 = \nu s_2 + \alpha g_1 - (\beta + k_{dd})g_2, \quad (3)$$

$$\partial_t g_3 = \nu s_3 - (\beta + k_{dd})g_3 + \alpha^* g_1.$$

Parameter ν in Eqs (3) represents the stem-cell mitotic rate, $\nu = 1$ per cell cycle.

The system of Eqs (2) and (3) was solved using VCell (www.vcell.org). The VCell implementation of the model can be found in the VCell database of public MathModels under username "boris"; the model name is "Inaba_dedifferentiation_model_public".

Model Parameters

We constrained model parameters using the results of long-term live imaging, along with the analysis of the model's salient features.

Not all parameters of the model are independent. Experimental observations indicate that by the time of eclosion, the pool of differentiated cells available for dedifferentiation has approached its steady-state size equaling N, i.e. $m_1(t) + m_2(t) + m_3(t) = N = const$ and $\sum_{j=1}^{3} g_j(t) = 1$. This makes the mechanism of replenishing of GSCs by dedifferentiation mathematically equivalent to symmetric renewal with an effective $q_{eff} = k_{dd} + q = r$ and $p + q_{eff} + r = \nu$. Indeed, from Eq (1), $\sum_{i=0}^{3} s_i(t) = 1$. Then summing up Eqs (2) yields $k_{dd} = \frac{(r-q)}{\sum_{j=1}^{3} g_j(t)} = r - q$, and since $\sum_{j=1}^{3} g_j(t) = 1$,

$$k_{dd} + q = r, \text{ and } p + 2\,r = \nu. \quad (4)$$

Eqs (4) are consistent with the data cited at the beginning of the section *Improvement of genetic marking system for identifying dedifferentiated GSCs*. Correspondingly, $p =$ 0.72/cycle and $k_{dd} =$ 0.1/cycle, then $r = \frac{1}{2}(\nu - p) =$ 0.14/cycle and $q = r - k_{dd} =$ 0.04/cycle.

Similarly, summing up Eqs (3) yields $\nu = \beta + k_{dd}$, and $\beta =$ 0.9/cycle.

Fitting the model to experimental data

To determine parameters α^{True} and α^*, we fitted our model to experimental time dependences of fractions of the GFP-positive GSCs obtained for a given genetic marker with an experimentally constrained ratio α^*/α^{true}. For this, Eqs (2) and (3) should be solved with varying α^{true} and initial conditions, to minimize the deviation between the solution of the model and the experimental data. As the experimental data are available beginning with the fly's eclosion, trying possible values of the seven model variables at the time of eclosion would be unwieldy. Instead, we moved the zero time point to the time in the larvae stage at which stem cells start to divide. It is reasonable to assume that at that time, all GCSs are unmarked, and the numbers of differentiated cells are zero. This allowed us to solve the model with same initial conditions in all trials and only vary the time of eclosion, τ_{ecl}. One caveat is that $k_{dd}(t) = \frac{(r-q)}{\sum_{j=1}^{3} g_j(t)}$ becomes now a function of time, since $\sum_{j=1}^{3} g_j(t)$ is not at steady state at $t \leq \tau_{ecl}$. To avoid division by zero in the equation for $k_{dd}(t)$, the initial conditions used in all our trials were as follows: $s_0(0) = 1$, $s_i(0) = 0$ $(i = 1,2,3)$, $g_0(0) = \varepsilon$, $g_j(0) = 0$ $(j = 2,3)$, where ε is a small number (in our simulations, $\varepsilon =$ 10^{-6}). The results were then offset by τ_{ecl} for comparison with the experimental data.

We characterized discrepancy between the simulation results and experimental data by the root-mean-square deviation (RMSD) defined as $\delta = (n^{-1}\sum_{i=1}^{n}(y_{exp}(t_i) - y_{theor}(t_i))^2)^{1/2}$, where n is the number of time points, for which we performed the comparison, $y_{exp}(t_i)$ are the

experimental values at times t_i, and $y_{theor}(t_i) = s_2(t_i) + s_3(t_i) \equiv s_+(t_i)$. Good fits, characterized by $\delta \sim$ 0.02-0.04, were obtained with $\tau_{ecl} =$ 6 cycles.

Once fully parameterized, the model was used to explore sensitivities of the marking systems to k_{dd} and α^{true}, and to compute the probability of false positives, $\frac{s_3(t)}{s_+(t)} = \frac{s_3(t)}{s_2(t) + s_3(t)}$.

Statistical analysis and graphing

No statistical methods were used to predetermine the sample size. The experiment values were not randomized. The investigators were not blinded to allocation during experiments and outcome assessment. All experiments were independently repeated at least 3 times to confirm the results. Statistical analysis and graphing were performed using GraphPad prism9. The illustrations were generated by using Adobe Illustrator or BioRender. All data are shown as means ± s.d.

Acknowledgments

We thank Yukiko M. Yamashita, Michael Buszczak and the Bloomington *Drosophila* Stock Center, and the Developmental Studies Hybridoma Bank for reagents. This research is supported by R35GM128678 from the National Institute for General Medical Sciences and start-up funds from UConn Health (to M.I.). B.M.S. was supported in part by R24GM137787 from National Institute for General Medical Sciences.

Author Contributions

M.I. and M.B.B. conceived the project, designed and executed experiments and analyzed data. B.M.S. and M.B.B. conducted mathematical modeling and data fitting using *Virtual Cell*. All authors wrote and edited the manuscript.

Declaration of Interests

The authors declare no competing interests.

503 **Figures**

504

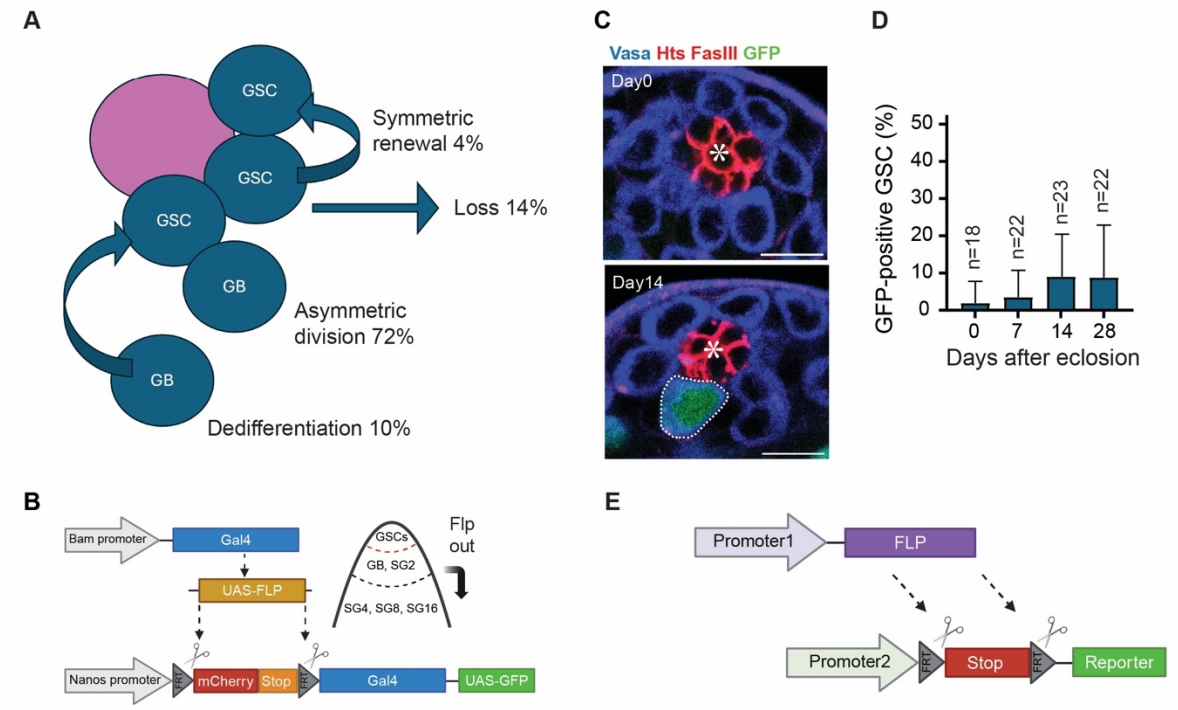

505
506
507
508
509
510
511
512
513
514
515
516
517
518
519
520
521
522
523
524
525
526
527
528
529

530 **Figure 1. Improvement of genetic marking system for identifying dedifferentiated GSCs.**
531 **A)** A schematic diagram illustrating the estimated rates of asymmetric division, symmetric
532 renewal, differentiation, and dedifferentiation of GSCs under steady-state conditions within the
533 testicular niche shown in our previous study [9]. **B)** An illustration of the bamGal4-driven FLP
534 lineage tracing system. The bamGal4 driver induces FLP expression in differentiating cells (4-
535 cell and later-stage SGs), where FLP excises the mCherry-stop cassette. If cells with the removed
536 stop cassette revert to the GSC state, they can be identified by the GFP expression under the
537 control of nosGal4 driver. **C**) Representative immunofluorescence images showing the testicular
538 niche in bamGal4-driven FLP lineage tracing system in the males at 0 and 14 days post-eclosion.
539 The testes were stained with Vasa (blue), FasIII (red), and Hts (red) antibodies. GFP-positive
540 GSCs (green) are encircled by white dotted lines. **D**) A graph showing the percentage of GFP-
541 positive GSCs per testis at 0, 7, 14, and 28 days post-eclosion. **E)** An illustration of the lineage
542 tracing system where FLP recombinase is directly expressed under a promoter and excises the
543 FRT sites from the reporter cassette. The reporter gene is expressed under a separate promoter.
544 All scale bars are 10 μm. Asterisks in the images indicate the approximate location of the hub.
545 "n" indicates the number of testes scored.

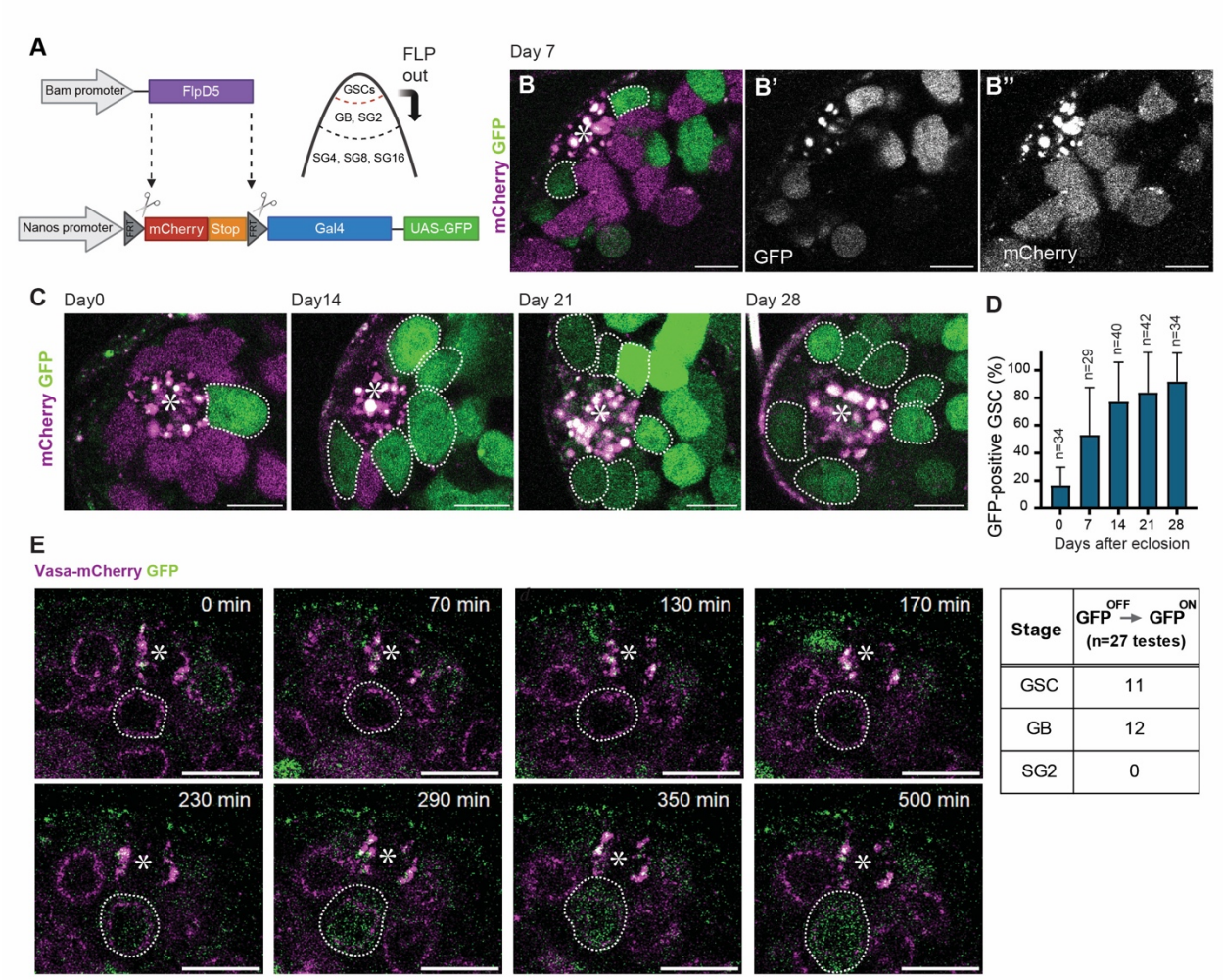

Stage	GFP^{OFF} → GFP^{ON} (n=27 testes)
GSC	11
GB	12
SG2	0

546
547
548
549

550 **Figure 2. Bam-FLPD5 causes spontaneous flipping events in GSCs, which obscures**
551 **dedifferentiation marking.**
552 **A)** An illustration of the Bam-FLPD5 lineage tracing system. Here, FLPD5 expression is driven
553 directly under the Bam promoter sequence (-198 to transcription start site, TSS) [45]. The Bam-
554 FLPD5 is crossed with nos-FRT-mCherry-stop-FRT-Gal4, UAS-GFP cassette (nos>>GFP) **B,**
555 **C**) Representative images of live testes of indicated ages of the Bam-FLPD5-driven lineage-
556 tracing system. GFP and mCherry channels are shown in separate panels in **B'** (for GFP) and **B''**
557 (for mCherry). **D)** A graph showing the scored percentage of GFP-positive GSCs per testis on
558 days 0, 7, 14, 21, and 28 post-eclosion. **E)** Selected frames of time-lapse images from a 12-hour
559 recording (interval:10min) of a niche showing the GFP-activation in a native GSC
560 (corresponding to Movie S1). Germline cells are visualized by expression of Vasa-mCherry
561 (magenta). White dotted lines encircle a GSC, becoming GFP-positive. Asterisks in the images
562 indicate the approximate location of the hub. The table (right panel) shows the number of times
563 GFP was observed to activate for each indicated cell stage (GSC, GB, and SG) during the 12-
564 hour live imaging recording of 27 testes.
565 All scale bars are 10 μm. Asterisks in the images indicate the approximate location of the hub.
566 "n" indicates the number of testes scored.
567
568
569
570
571
572
573
574
575
576

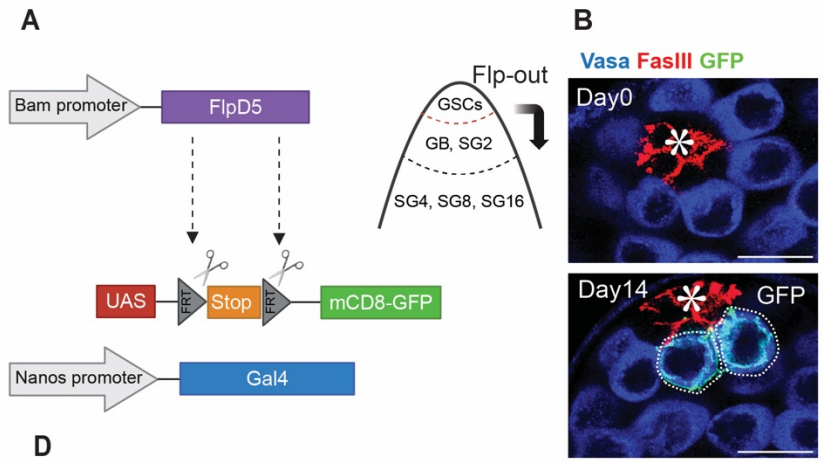

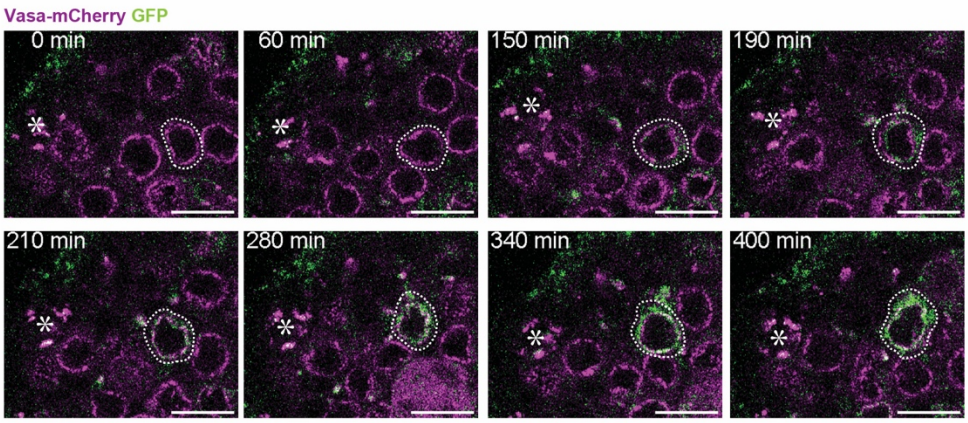

Stage	GFP^{OFF} → GFP^{ON} (n=25 testes)
GSC	1
GB	12
SG2	4

577
578

579 **Figure 3. UAS-FRT-stop-FRT-mCD8-GFP cassette is efficiently flipped in GB/SGs but not**
580 **in GSCs.**
581 **A)** An illustration of the Bam-FLPD5 lineage tracing system. Here, Bam-FLPD5 is combined
582 with the UAS-FRT-stop-FRT-mCD8-GFP cassette and nosGal4 (nos>>mCD8GFP). FLPD5
583 removes the stop codon from this cassette. If cells once removed stop cassette in the past become
584 GSCs, they can be identified by the GFP expression under the control of nosGal4 driver. **B)**
585 Representative immunofluorescence images of the testicular niche of the Bam-FLPD5 marking
586 system in the males at 0 and 14 days post-eclosion. The testes were stained with Vasa (blue) and
587 FasIII (red) antibodies. GFP-positive GSCs (green) are outlined by white dotted lines. **C)** A
588 graph showing the percentage of GFP-positive GSCs per testis at 0, 7, 14, and 28 days post-
589 eclosion. **D)** Selected frames from a 12-hour time-lapse recording (interval:10 min) of a niche
590 showing the GFP-activation in a GB (corresponding to Movie S2). Germline cells are visualized
591 by expression of Vasa-mCherry (magenta). White dotted lines encircle a GB becoming GFP
592 positive. The table (right panel) shows the number of times GFP was observed to activate for
593 each indicated cell stage (GSC, GB, and SG) during 12-hour live imaging recording of 25 testes.
594 All scale bars are 10 μm. Asterisks in the images indicate the approximate location of the hub.
595 "n" indicates the number of testes scored.
596
597
598
599
600
601
602
603
604
605
606
607
608
609
610
611
612
613
614
615

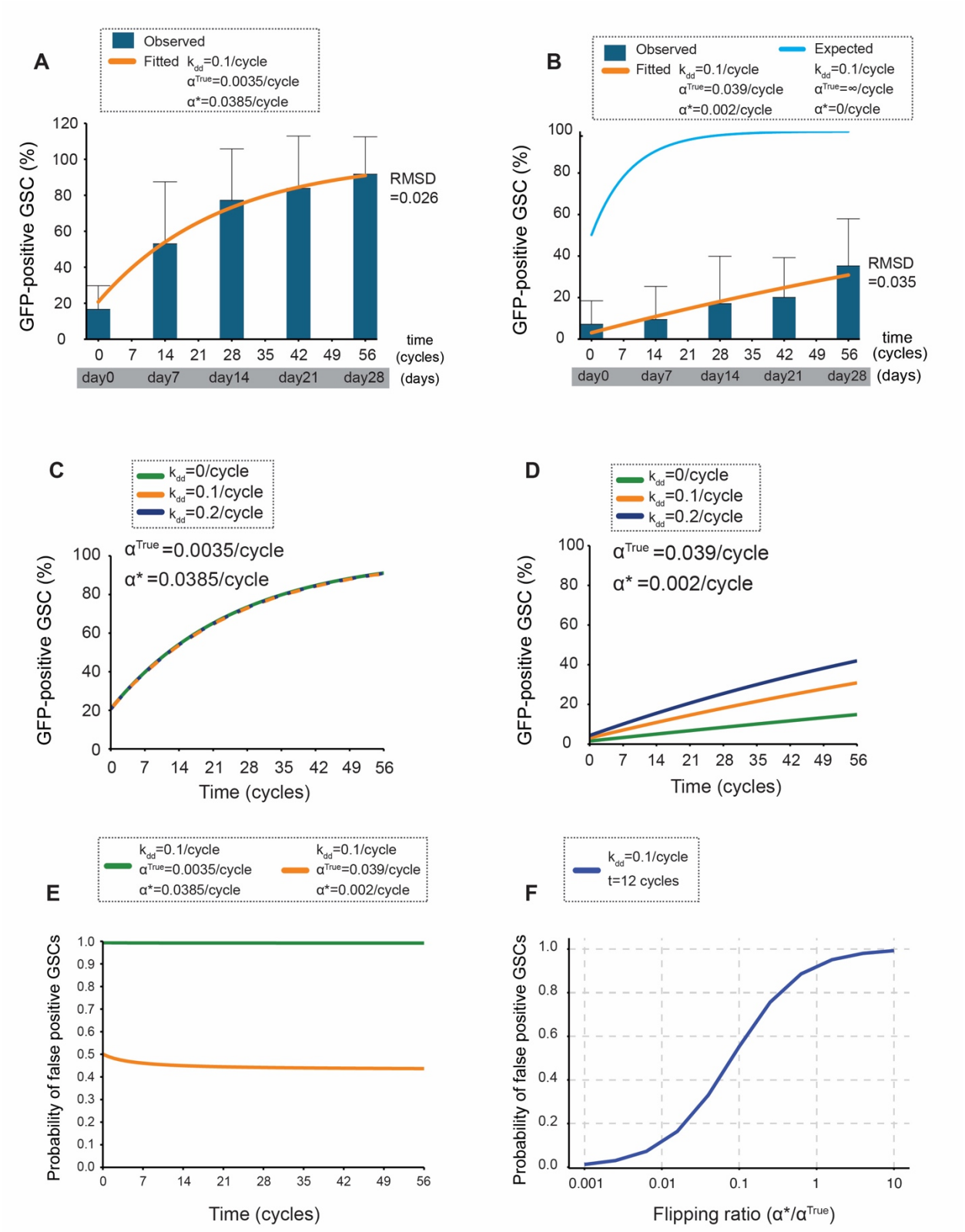

616
617
618
619

Figure 4. Quantifying specificity and efficiency of lineage marking

A) Model fitting for the Bam-FLPD5, nos>>GFP system. Experimental data showing the percentage of GFP-positive GSCs over time (blue bars; data from Figure 2D) are compared to the best-fit model output (orange curve). The model incorporates key cellular processes (see Figure S1A, B and Materials and Methods for details). The root mean squared deviation (RMSD) between the model and the experimental data is 0.026. Two cycles are equivalent to one day [46]. Fitted parameters (α^{True} and α^*) are shown in the graph. See Source Data file for numerical values and all parameter values.

B) Model fitting for the Bam-FLPD5, nos>>mCD8GFP system. Experimental data showing the percentage of GFP-positive GSCs over time (blue bars; data from Fig 3C) are compared to the best-fit model output (orange curve). The root mean squared deviation (RMSD) between the model and the experimental data is 0.035. The blue line represents the expected percentage of GFP-positive GSCs if the recombination efficiency was 100% in all differentiating cells ($\alpha^{True}=\infty$) and with no spontaneous GFP activation ($\alpha^*=0$)

C) Predicted effect of dedifferentiation rate (k_{dd}) on GFP-positive GSCs in the Bam-FLPD5, nos>>GFP system. Model predictions for the percentage of GFP-positive GSCs over time are shown for different dedifferentiation rates (k_{dd} = 0, 0.1, and 0.2 per cell cycle). The overlapping lines demonstrate that the system is insensitive to changes in k_{dd} due to high ratio of α^*/α^{True} = 11.

D) Predicted effect of dedifferentiation rate (k_{dd}) on GFP-positive GSCs in the Bam-FLPD5, nos>>mCD8GFP system. Model predictions for the percentage of GFP-positive GSCs over time are shown for different dedifferentiation rates (k_{dd} = 0, 0.1, and 0.2 per cell cycle). The lines demonstrate the system's sensitivity to changes in k_{dd} due to lower ratio of α^*/α^{True} = 0.0667.

E) Predicted probability of false positive GSCs over time. The model-predicted probabilities of a GFP-positive GSC being a false positive are shown for the Bam-FLPD5, nos>>GFP system (green line) and the Bam-FLPD5, nos>>mCD8GFP system (orange line). The nos>>GFP system shows a near 100% false positive probability, while the nos>>mCD8GFP system shows a significantly lower probability of approximately 45%.

F) Predicted probability of false positive GSCs as a function of the flipping ratio over time for two different marking systems with varying flipping ratios (α^*/α^{True}). The analysis was performed at a representative time point (t=12 cycles).

651

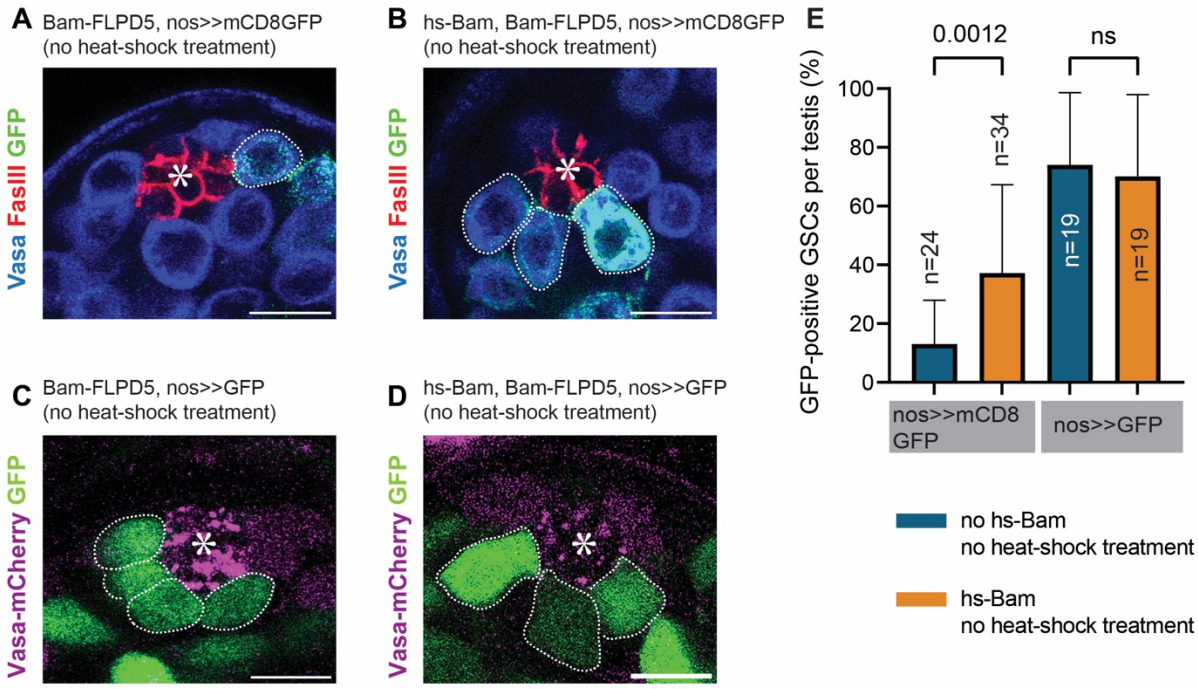

652
653
654

Figure 5. Introduction of a hs-Bam transgene results in high frequency of marked GSCs

A, B) Representative immunofluorescence images of the testis tip from 7-day-old flies with Bam-FLPD5 marking system with the nos>>mCD8GFP cassette alone **(A)** or with an additional single copy of the hs-Bam transgene **(B)**. Testes were stained with Vasa (blue) and FasIII (red) antibodies. GFP-positive GSCs (green) are outlined with white dotted lines.

C, D) Representative images of live testis tip from 7-day-old flies with Bam-FLPD5 marking system with the nos>>GFP cassette alone **(C)** or a combination with a single copy of hs-Bam **(D)**.

E) The graph shows the quantification of GFP-positive GSCs per testis in 7-day-old flies without heat-shock treatment for the indicated genotypes.

All scale bars are 10 µm. Asterisks in the images indicate the approximate location of the hub. p-values were calculated by Šídák's multiple comparisons test. “n” indicates the number of testes scored.

694 **References**
695

696 1. Brawley, C. and E. Matunis, *Regeneration of male germline stem cells by spermatogonial*
697 *dedifferentiation in vivo.* Science, 2004. **304**(5675): p. 1331-4.
698 2. Liu, Y. and Y.G. Chen, *Intestinal epithelial plasticity and regeneration via cell*
699 *dedifferentiation.* Cell Regen, 2020. **9**(1): p. 14.
700 3. Sun, Q., et al., *Dedifferentiation maintains melanocyte stem cells in a dynamic niche.*
701 Nature, 2023. **616**(7958): p. 774-782.
702 4. Tata, P.R., et al., *Dedifferentiation of committed epithelial cells into stem cells in vivo.*
703 Nature, 2013. **503**(7475): p. 218-223.
704 5. Tetteh, Paul W., et al., *Replacement of Lost Lgr5-Positive Stem Cells through Plasticity of*
705 *Their Enterocyte-Lineage Daughters.* Cell Stem Cell, 2016. **18**(2): p. 203-213.
706 6. Murata, K., et al., *Ascl2-Dependent Cell Dedifferentiation Drives Regeneration of Ablated*
707 *Intestinal Stem Cells.* Cell Stem Cell, 2020. **26**(3): p. 377-390.e6.
708 7. Merrell, A.J. and B.Z. Stanger, *Adult cell plasticity in vivo: de-differentiation and*
709 *transdifferentiation are back in style.* Nat Rev Mol Cell Biol, 2016. **17**(7): p. 413-25.
710 8. Kai, T. and A. Spradling, *Differentiating germ cells can revert into functional stem cells in*
711 *Drosophila melanogaster ovaries.* Nature, 2004. **428**(6982): p. 564-569.
712 9. Bener, M.B., A. Twillie, and M. Inaba, *Dedifferentiating germ cells regain stem-cell*
713 *specific polarity checkpoint prior to niche reentry.* bioRxiv, 2023: p. 2023.04.26.538507.
714 10. Herrera, S.C. and E.A. Bach, *JNK signaling triggers spermatogonial dedifferentiation*
715 *during chronic stress to maintain the germline stem cell pool in the Drosophila testis.*
716 eLife, 2018. **7**: p. e36095.
717 11. Cheng, J., et al., *Centrosome misorientation reduces stem cell division during ageing.*
718 Nature, 2008. **456**(7222): p. 599-604.
719 12. Malagola, E., et al., *Isthmus progenitor cells contribute to homeostatic cellular turnover*
720 *and support regeneration following intestinal injury.* Cell, 2024. **187**(12): p. 3056-
721 3071.e17.
722 13. Nagai, H., et al., *Nutrient-driven dedifferentiation of enteroendocrine cells promotes*
723 *adaptive intestinal growth in Drosophila.* Developmental Cell, 2023. **58**(18): p. 1764-
724 1781.e10.
725 14. Van Es, J.H., et al., *Dll1+ secretory progenitor cells revert to stem cells upon crypt*
726 *damage.* Nature cell biology, 2012. **14**(10): p. 1099-1104.
727 15. Álvarez-Aznar, A., et al., *Tamoxifen-independent recombination of reporter genes limits*
728 *lineage tracing and mosaic analysis using CreER(T2) lines.* Transgenic Res, 2020. **29**(1): p.
729 53-68.
730 16. Fuller, M.T. and A.C. Spradling, *Male and female Drosophila germline stem cells: two*
731 *versions of immortality.* Science, 2007. **316**(5823): p. 402-4.
732 17. Greenspan, L.J., M. de Cuevas, and E. Matunis, *Genetics of gonadal stem cell renewal.*
733 Annu Rev Cell Dev Biol, 2015. **31**: p. 291-315.
734 18. Yamashita, Y.M., D.L. Jones, and M.T. Fuller, *Orientation of asymmetric stem cell division*
735 *by the APC tumor suppressor and centrosome.* Science, 2003. **301**(5639): p. 1547-50.
736 19. de Cuevas, M. and E.L. Matunis, *The stem cell niche: lessons from the Drosophila testis.*
737 Development, 2011. **138**(14): p. 2861-9.

20. Nern, A., et al., *Multiple new site-specific recombinases for use in manipulating animal genomes.* Proceedings of the National Academy of Sciences, 2011. **108**(34): p. 14198-14203.
21. Cherry, C.M. and E.L. Matunis, *Epigenetic regulation of stem cell maintenance in the Drosophila testis via the nucleosome-remodeling factor NURF.* Cell Stem Cell, 2010. **6**(6): p. 557-67.
22. Insco, M.L., et al., *Accumulation of a differentiation regulator specifies transit amplifying division number in an adult stem cell lineage.* Proceedings of the National Academy of Sciences, 2009. **106**(52): p. 22311-22316.
23. Salzmann, V., et al., *Lineage tracing quantification reveals symmetric stem cell division in Drosophila male germline stem cells.* Cell Mol Bioeng, 2013. **6**(4): p. 441-448.
24. Bener, M.B., B.M. Slepchenko, and M. Inaba, *Asymmetric stem cell division maintains the genetic heterogeneity of tissue cells.* bioRxiv, 2024: p. 2024.05.16.594576.
25. Resasco, D.C., et al., *Virtual Cell: computational tools for modeling in cell biology.* Wiley Interdiscip Rev Syst Biol Med, 2012. **4**(2): p. 129-40.
26. Slepchenko, B.M. and L.M. Loew, *Use of virtual cell in studies of cellular dynamics.* Int Rev Cell Mol Biol, 2010. **283**: p. 1-56.
27. Sheng, X.R., C.M. Brawley, and E.L. Matunis, *Dedifferentiating Spermatogonia Outcompete Somatic Stem Cells for Niche Occupancy in the Drosophila Testis.* Cell Stem Cell, 2009. **5**(2): p. 191-203.
28. Payne, S., S. De Val, and A. Neal, *Endothelial-Specific Cre Mouse Models.* Arteriosclerosis, Thrombosis, and Vascular Biology, 2018. **38**(11): p. 2550-2561.
29. Magnuson, M.A. and A.B. Osipovich, *Pancreas-specific Cre driver lines and considerations for their prudent use.* Cell metabolism, 2013. **18**(1): p. 9-20.
30. Nakagawa, T., et al., *Functional hierarchy and reversibility within the murine spermatogenic stem cell compartment.* Science, 2010. **328**(5974): p. 62-67.
31. Sheng, X.R. and E. Matunis, *Live imaging of the Drosophila spermatogonial stem cell niche reveals novel mechanisms regulating germline stem cell output.* Development, 2011. **138**(16): p. 3367-76.
32. Wu, S.S., J.H. Lee, and B.K. Koo, *Lineage Tracing: Computational Reconstruction Goes Beyond the Limit of Imaging.* Mol Cells, 2019. **42**(2): p. 104-112.
33. Wagner, D.E. and A.M. Klein, *Lineage tracing meets single-cell omics: opportunities and challenges.* Nature Reviews Genetics, 2020. **21**(7): p. 410-427.
34. Pei, W., et al., *Polylox barcoding reveals haematopoietic stem cell fates realized in vivo.* Nature, 2017. **548**(7668): p. 456-460.
35. Pei, W., et al., *Using Cre-recombinase-driven Polylox barcoding for in vivo fate mapping in mice.* Nature Protocols, 2019. **14**(6): p. 1820-1840.
36. Ludwig, L.S., et al., *Lineage Tracing in Humans Enabled by Mitochondrial Mutations and Single-Cell Genomics.* Cell, 2019. **176**(6): p. 1325-1339.e22.
37. Kalhor, R., et al., *Developmental barcoding of whole mouse via homing CRISPR.* Science, 2018. **361**(6405).
38. Yamashita, Y.M., *Nonrandom sister chromatid segregation of sex chromosomes in Drosophila male germline stem cells.* Chromosome Research, 2013. **21**(3): p. 243-254.

39. Tran, V., et al., *Asymmetric division of Drosophila male germline stem cell shows asymmetric histone distribution.* Science, 2012. **338**(6107): p. 679-82.
40. Yamashita, Y.M., et al., *Asymmetric inheritance of mother versus daughter centrosome in stem cell division.* Science, 2007. **315**(5811): p. 518-21.
41. Schwitalla, S., et al., *Intestinal tumorigenesis initiated by dedifferentiation and acquisition of stem-cell-like properties.* Cell, 2013. **152**(1-2): p. 25-38.
42. Friedmann-Morvinski, D., et al., *Dedifferentiation of neurons and astrocytes by oncogenes can induce gliomas in mice.* Science, 2012. **338**(6110): p. 1080-4.
43. Van Doren, M., A.L. Williamson, and R. Lehmann, *Regulation of zygotic gene expression in Drosophila primordial germ cells.* Curr Biol, 1998. **8**(4): p. 243-6.
44. Lerit, D.A. and E.R. Gavis, *Transport of germ plasm on astral microtubules directs germ cell development in Drosophila.* Curr Biol, 2011. **21**(6): p. 439-48.
45. Ridwan, S.M., et al., *Diffusible fraction of niche BMP ligand safeguards stem-cell differentiation.* Nature Communications, 2024. **15**(1): p. 1166.
46. Gadre, P., et al., *The rates of stem cell division determine the cell cycle lengths of its lineage.* iScience, 2021. **24**(11): p. 103232.